



Cite this: *Org. Biomol. Chem.*, 2020, **18**, 154

From simple quinoxalines to potent oxazolo[5,4-*f*]quinoxaline inhibitors of glycogen-synthase kinase 3 (GSK3)[†]

Frédéric Lassagne,^a Camille Duguépéroux,^a Carlos Roca,^b Concepcion Perez,^c Ana Martinez,^{b,d} Blandine Baratte,^{e,f} Thomas Robert,^{e,f} Sandrine Ruchaud,^{e,f} Stéphane Bach,^{e,f} William Erb,^a Thierry Roisnel^a and Florence Mongin^a

2,7-Disubstituted oxazolo[5,4-*f*]quinoxalines were synthesized from 6-amino-2-chloroquinoxaline in four steps (iodination at C5, substitution of the chloro group, amidation and copper-catalysed cyclization) affording 28 to 44% overall yields. 2,8-Disubstituted oxazolo[5,4-*f*]quinoxaline was similarly obtained from 6-amino-3-chloroquinoxaline (39% overall yield). For the synthesis of other oxazolo[5,4-*f*]quinoxalines, amidation was rather performed before substitution; moreover, time-consuming purification steps were avoided between the amines and the final products (38 to 54% overall yields). Finally, a more efficient method involving merging of the last two steps in a sequential process was developed to access more derivatives (37 to 65% overall yields). Most of the oxazolo[5,4-*f*]quinoxalines were evaluated for their activity on a panel of protein kinases, and a few 2,8-disubstituted derivatives proved to inhibit GSK3 kinase. While experiments showed an ATP-competitive inhibition on GSK3 β , structure–activity relationships allowed us to identify 2-(3-pyridyl)-8-(thiomorpholino)oxazolo[5,4-*f*]quinoxaline as the most potent inhibitor with an IC₅₀ value of about 5 nM on GSK3 α .

Received 12th September 2019,
Accepted 27th November 2019

DOI: 10.1039/c9ob02002k

rsc.li/obc

Introduction

Oxazolo[5,4-*f*]quinoxalines, to our knowledge, have never been synthesized before. Their structures can be seen either as a pyrazine fused to a benzoxazole or as an oxazole fused to a quinoxaline¹ (Fig. 1, top left). Oxazolo[4,5-*h*]quinolines, which are analogues of oxazolo[5,4-*f*]quinoxalines, lacking one nitrogen (Fig. 1, top right), have shown anti-allergic activities.² Thus, it is of interest to access oxazolo[5,4-*f*]quinoxalines and

study their biological behaviour in order to find original properties.

It has been shown in 2011 that 2-quinolinol can be functionalized either at its 6- or at its 7-position by nitration at room temperature using potassium nitrate in sulfuric acid or nitric acid in acetic acid, respectively.³ Subsequent conversion to the corresponding chlorides (reflux with phosphorus oxychloride and phosphorus pentachloride) and nitro reduction³ can easily furnish appropriate substrates (Fig. 1, bottom) for the synthesis of various 2,7- and 2,8-disubstituted oxazolo[5,4-*f*]quinoxalines.

Recently, our random screening of original polyaromatic compounds revealed inhibitors of protein kinases.⁴ Following

^aUniv Rennes, CNRS, ISCR (Institut des Sciences Chimiques de Rennes) – UMR 6226, F-35000 Rennes, France. E-mail: florence.mongin@univ-rennes1.fr

^bCentro de Investigaciones Biológicas-CSIC, Ramiro de Maeztu 9, 28040 Madrid, Spain. E-mail: ana.martinez@csic.es

^cInstituto de Química Médica-CSIC, Juan de la Cierva 3, 28006 Madrid, Spain

^dCentro de Investigación Biomédica en Red de Enfermedades Neurodegenerativas (CIBERNED), Instituto Carlos III, 28031 Madrid, Spain

^eSorbonne Université, CNRS, FR2424, Plateforme de criblage KISSf (Kinase Inhibitor Specialized Screening facility), Station Biologique de Roscoff, CS 90074, 29682 Roscoff Cedex, France. E-mail: bach@sb-roscoff.fr

^fSorbonne Université, CNRS, UMR 8227, Integrative Biology of Marine Models, Station Biologique de Roscoff, CS 90074, 29688 Roscoff Cedex, France

[†]Electronic supplementary information (ESI) available: General information, experimental procedures and analyses of the compounds and NMR spectra. CCDC 1947178 (10ba) and 1964834 (10ci). For ESI and crystallographic data in CIF or other electronic format see DOI: 10.1039/c9ob02002k

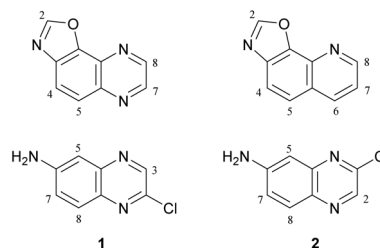


Fig. 1 Top: Structures of oxazolo[5,4-*f*]quinoxaline (left) and oxazolo[4,5-*h*]quinoline (right). Bottom: Planned quinoxaline substrates.

these studies, we report in the present paper the synthesis of original oxazolo[5,4-*f*]quinoxalines and evaluation of their activity on a panel of protein kinases. Docking studies are carried out, leading to a potent inhibitor of GSK3.

Results and discussion

6-Amino-2-chloroquinoxaline (**1**) was converted into 2,7-disubstituted oxazolo[5,4-*f*]quinoxalines in four steps (Scheme 1). An approach to obtain benzoxazole is by constructing a ring from 2-haloanilide.⁵ Therefore, inspired by the reported bromination of 6-aminoquinoxaline at C5,⁶ we treated a solution of **1** in 4 : 1 dioxane–water with an excess of iodine and sodium bicarbonate at room temperature for 4 h. Under these conditions, the 5-iodo derivative **3**, formed regioselectively, was isolated in 88% yield.

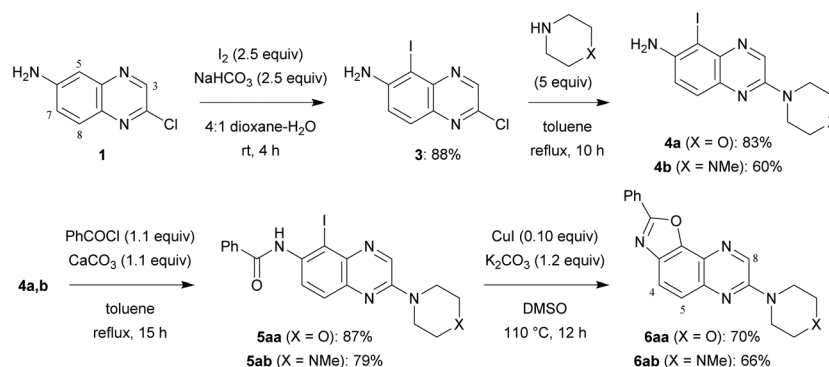
In order to progress towards compounds of biological interest, the chloro group was successfully replaced by morpholino and 4-methylpiperazino at the reflux temperature of toluene, affording **4a,b**. Their reaction with benzoyl chloride in the presence of calcium carbonate under similar conditions led to benzamides **5aa** and **5ab**.

Next, we sought simple and efficient conditions under which we could attempt the synthesis of benzoxazole.^{5,7} Convinced with the interest in copper-catalysed reactions, we decided to use catalytic copper(i) iodide in the presence of pot-

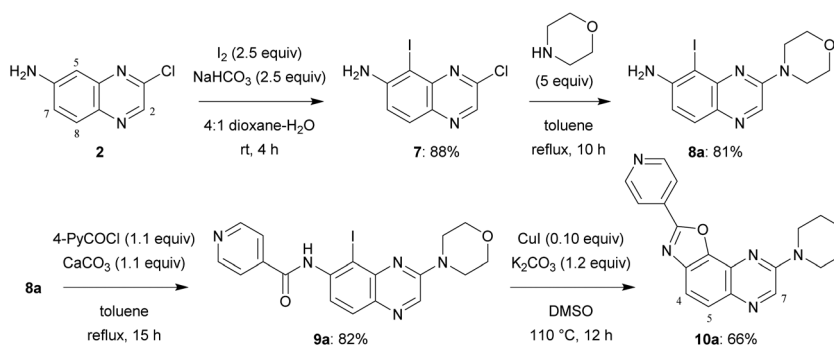
assium carbonate, and selected dimethylsulfoxide as the solvent in order to avoid an additional ligand. As expected, after 12 h at 110 °C, 2,7-disubstituted oxazolo[5,4-*f*]quinoxalines **6aa** and **6ab** were isolated in good yields.

A similar four-step synthesis, employing isonicotinoyl chloride instead of benzoyl chloride, was used to obtain 2,8-disubstituted oxazolo[5,4-*f*]quinoxaline **10a** (Scheme 2).

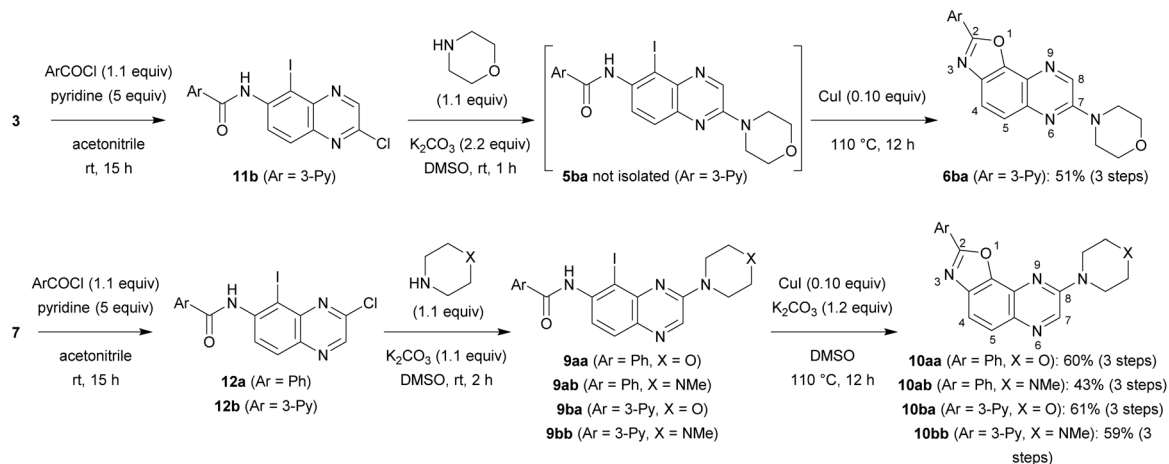
For the purpose of moving towards a more convergent strategy, we reversed the order of the steps and performed amidation before substitution of the chloro group (Scheme 3). A further benefit of this approach would be the possibility to carry out substitution under milder conditions; indeed, the reaction should be favoured with a less electron-donating group such as aroylamino at C6 than the previous amino group. In a preliminary attempt, iodide **3** was treated with nicotinoyl chloride; to solve the solubility issue sometimes encountered with toluene, acetonitrile containing 5 equivalents of pyridine was rather employed. Next, chlorocarboxamide **11b** was reacted with morpholine in dimethylsulfoxide, a solvent also suitable for the formation of benzoxazole, and an excess of potassium carbonate was introduced right from the beginning of the reaction. After the required time to achieve nucleophilic substitution at room temperature, catalytic copper(i) iodide was introduced and the mixture containing **5ba** was heated to 110 °C in order to allow cyclization to take place. Under these conditions, 2,7-disubstituted oxazolo[5,4-*f*]quinoxaline **6ba** was isolated after



Scheme 1 Synthesis of 2,7-disubstituted oxazolo[5,4-*f*]quinoxalines **6aa** and **6ab**.



Scheme 2 Synthesis of 2,8-disubstituted oxazolo[5,4-*f*]quinoxaline **10a**.



Scheme 3 Synthesis of 2,7-disubstituted oxazolo[5,4-*f*]quinoxalines **6ba** and 2,8-disubstituted oxazolo[5,4-*f*]quinoxalines **10aa**, **10ab**, **10ba** and **10bb**.

purification with an overall yield of 51% in this three-step process (Scheme 3, top).

In a similar way, iodide **7** was readily converted into carboxamide **12a,b** using either benzoyl chloride or nicotinoyl chloride. Further replacement of the chloro group by morpholino or 4-methylpiperazino benefited from the higher reactivity of **12a, b** towards nucleophiles when compared with **11b**. From the compounds **9aa**, **9ab**, **9ba** and **9bb**, here only isolated from their reaction mixture by a simple work-up to ascertain their formation by NMR, cyclization was performed, leading to the new 2,8-disubstituted oxazolo[5,4-*f*]quinoxalines **10aa**, **10ab**, **10ba** (unambiguously identified by X-ray diffraction; the corresponding ORTEP diagram is given in Fig. 2) and **10bb** (Scheme 3, bottom). It is worth noting that there is no need to purify the intermediates of this three-step synthesis process

from **7** as, after a suitable work-up, they can be directly involved in the substitution reaction and benzoxazole formation.

Protein kinases can be deregulated in diseases such as cancers and neurodegenerative disorders.⁸ Since the end of the nineties, this class of signalling biomolecules has become indispensable drug targets. As a result, many candidates are at present undergoing clinical evaluation and 50 FDA-approved kinase inhibitors are already in the market.⁹

In continuation of our ongoing research on novel protein kinase inhibitors,⁴ most of the synthesized oxazolo[5,4-*f*]quinoxalines as well as a few precursors were tested against a short panel of disease-related protein kinases: cyclin-dependent kinases 2 (CDK2/CyclinA), 5 (CDK5/p25) and 9 (CDK9/CyclinT), proto-oncogene kinase PIM1, CDC2-like kinase 1 (CLK1), dual specificity tyrosine phosphorylation regulated kinase 1A (DYRK1A), glycogen synthase kinase 3 (GSK3; isoform β , and possibly α or/and α/β), casein kinase 1 (CK1; isoform ϵ , and possibly δ/ϵ) and mitotic kinase Haspin (Table 1).

Interestingly, some of the oxazolo[5,4-*f*]quinoxalines and, to a lesser extent, their non-cyclized precursors proved to significantly inhibit CDK9/CyclinT, DYRK1A and GSK3 at 10 μ M. In addition, even at a lower concentration of 1 μ M, compounds **10ba** and **10bb** bearing a 3-pyridyl ring at C2 still exhibit good activity against GSK3 protein kinase. IC₅₀ values were calculated for the most promising compounds; while micromolar values for GSK3 inhibition were found in the case of **10aa** and **10ab**, encouraging submicromolar values were recorded for **10ba** and **10bb** (Table 2).

Because of its association with key biological processes (metabolism, cell signalling, cellular transport, apoptosis, proliferation, intracellular communication, *etc.*), the serine-threonine protein kinase GSK3 is implicated in various diseases (type 2 diabetes, bipolar disorder, schizophrenia, Alzheimer's disease, Parkinson's disease, developmental disorders and cancer), and has become an important target for drug development.¹⁰ Thus, our preliminary results prompted us to identify both the binding site and the binding mode of our best inhibi-

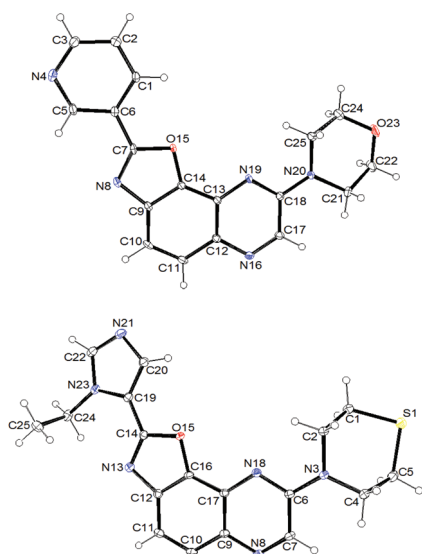


Fig. 2 ORTEP diagrams (30% probability) of **10ba** (top) and **10ci** (bottom).

Table 1 Inhibitory activities of the first round of compounds against a short panel of disease-related protein kinases. The table displays the remaining kinase activities detected after treatment with 10 μM of the tested compounds. The values obtained after treatment with 1 μM are given in brackets. Results are expressed in % of maximal activity, i.e. measured in the absence of the inhibitor but with an equivalent dose of DMSO (solvent of the tested compounds). ATP concentration used in the kinase assays was 10 $\mu\text{mol L}^{-1}$ (values are mean values, $n = 2$). Kinases are from human origin unless specified: Mm, *Mus musculus*; Rn, *Rattus norvegicus*; Ssc, *Sus scrofa domestica*

Compd.	CDK2/CyclinA	CDK5/p25	CDK9/CyclinT	PIM1	MmCLK1	RnDYRK1A	GSK3 α	GSK3 β	SscGSK3 α/β	CK1 ϵ	SscCK1 δ/ϵ	Haspin
5aa	—	≥ 100 (99)	90 (80)	100 (91)	91 (95)	100 (97)	—	89 (92)	—	92 (90)	—	77 (87)
5ab	—	≥ 100 (100)	84 (79)	≥ 100 (≥ 100)	59 (90)	89 (96)	—	76 (92)	—	73 (82)	—	68 (72)
6aa	—	100 (≥ 100)	93 (81)	≥ 100 (≥ 100)	59 (99)	84 (93)	—	96 (86)	—	83 (92)	—	57 (60)
6ab	—	≥ 100 (98)	72 (79)	≥ 100 (≥ 100)	44 (95)	73 (99)	—	89 (82)	—	86 (78)	—	64 (82)
6ba	—	≥ 100 (≥ 100)	≥ 100 (≥ 100)	99 (≥ 100)	—	70 (92)	≥ 100 (≥ 100)	90 (≥ 100)	—	81 (≥ 100)	—	87 (≥ 100)
9a	—	≥ 100 (≥ 100)	69 (73)	≥ 100 (≥ 100)	—	50 (72)	41 (72)	54 (64)	—	76 (88)	—	79 (≥ 100)
10a	—	≥ 100 (99)	52 (79)	78 (90)	—	42 (74)	24 (55)	51 (60)	—	72 (≥ 100)	—	59 (64)
9aa	48 (87)	96 (91)	25 (80)	84 (96)	—	—	33 (82)	37 (82)	43 (92)	78 (98)	—	—
10aa	70 (99)	≥ 100 (98)	40 (65)	97 (94)	—	—	13 (52)	33 (59)	29 (56)	85 (≥ 100)	—	—
10ab	52 (98)	85 (81)	4 (61)	75 (89)	—	—	≤ 0 (54)	12 (58)	14 (69)	40 (94)	—	—
10ba	—	66 (98)	27 (45)	23 (43)	—	3 (11)	9 (9)	2 (2)	—	65 (75)	—	12 (23)
10bb	≥ 100 (≥ 100)	93 (≥ 100)	7 (35)	20 (57)	—	—	2 (4)	6 (6)	16 (16)	53 (≥ 100)	72 (88)	24 (29)

Table 2 Selected IC₅₀ values (nM) for compounds in Table 1

Entry	Product	CDK9/CyclinT	GSK3 α	GSK3 β	SscGSK3 α/β
1	9aa	2500	2200	6800	8800
2	10aa	>10000	610	980	1100
3	10ab	3100	1600	3100	1900
4	10ba	—	15	25	—
5	10bb	—	24	55	30

tors **10ba** and **10bb** through (i) ATP-competition experiments and (ii) docking studies in order to optimize their structure.

(i) The kinetic mechanism of GSK3 β inhibition was experimentally investigated for one of the most potent derivatives synthesized, quinoxaline **10bb**, by varying the concentrations of both ATP and the tested inhibitor in the kinase reaction. The Lineweaver–Burk or double-reciprocal plots of $1/v$ versus $1/[\text{ATP}]$ at fixed concentrations of the new inhibitor **10bb** showed an intersecting pattern consistent with competitive inhibition as all lines converge at or near the y-axis (Fig. 3). These results clearly show that this new family of quinoxaline derivatives and specifically compound **10bb** are ATP-competitive GSK3 β inhibitors because an increase in the ATP concentration (from 1 to 100 μM) does not interfere with enzyme inhibition.

(ii) In order to develop structure–activity relationships and propose novel substituents able to increase kinase inhibition potency, we performed docking studies in the ATP-binding cavity of GSK3 β for compounds **10ab** and **10bb**. Both compounds are able to bind to the cavity through an H-bond interaction between the N6 atom of the oxazolo quinoxaline ring (see Scheme 3 for numbering) and the backbone amine group of Val135 (Fig. 4), orienting the substituent at C2 to the catalytic residue Lys85 and the substituent at C8 to the solvent. The main difference between both compounds is the substituent at C2, a phenyl ring (compound **10ab**) and a pyridine ring (compound **10bb**). The pyridine ring is able to interact through

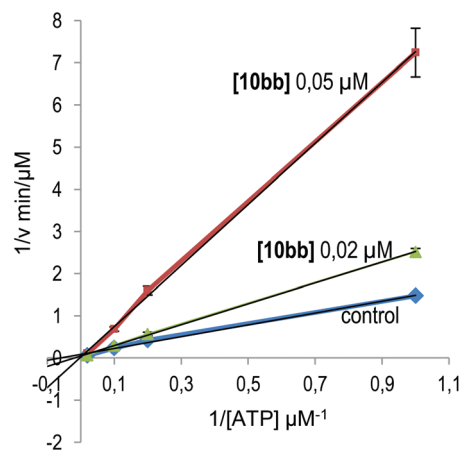


Fig. 3 Kinetic data determined for derivative **10bb**. ATP concentrations in the reaction mixture varied from 1 to 100 μM . Compound concentrations used are depicted in the plot, and the concentration of the substrate was kept constant at 12.5 μM . Each point is the mean of two different experiments, each one analysed in duplicate.

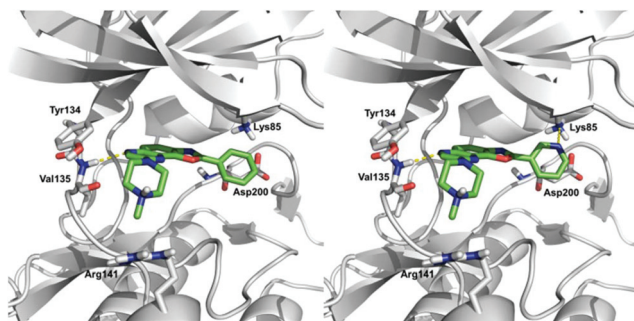


Fig. 4 Proposed binding mode for compounds **10ab** (left) and **10bb** (right) in the ATP binding pocket of GSK3 β .

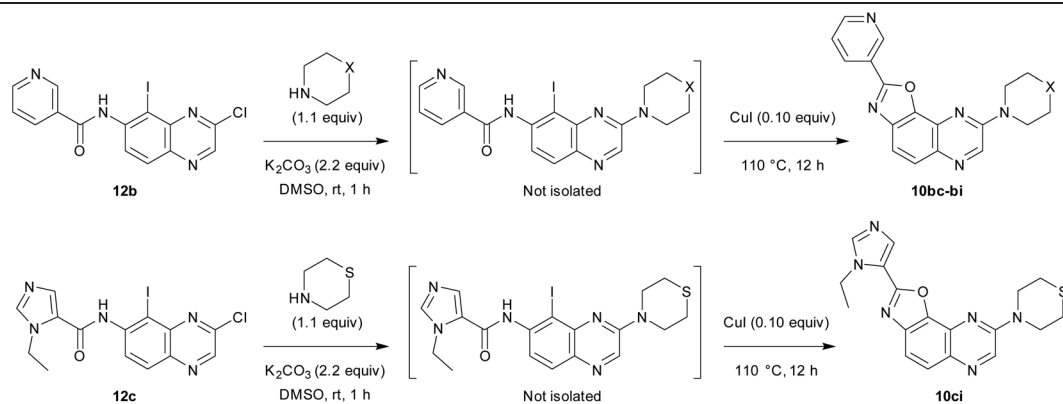
an H-bond interaction with Lys85, increasing the affinity and improving the inhibition of the target. Thus, in order to access more potent inhibitors, we could maintain the pyridine ring or replace it with a five-membered heterocycle that allows similar interaction. The substituent at C8 in both cases is a piperazine ring that is oriented to the solvent-exposed region. This orientation allows the introduction of different substituents in order to grow the ligand in this region. Moreover, substituents at this position with aromatic rings could be interesting to allow interaction with Arg141 through a π -cation interaction. Furthermore, H-bond acceptor groups at this position would also be able to interact with Arg141.

We first decided to keep the pyridine ring at C2 and replace the morpholine or 4-methylpiperazine present at C8 with various cyclic amines (Table 3, top scheme). To access the planned structures, we applied the procedure involving the merging of substitution and cyclization to obtain benzoxazole in a sequential process (Scheme 3, top). Indeed, we observed in the course of synthesis of **6ba** that there was no need to isolate intermediate **5ba** and to purify precursor **11b**. Thus, under these conditions, 2,8-disubstituted oxazolo[5,4-*f*]quinoxalines **10bc–bi** were prepared from the dihalogenated carboxamide **12b** and isolated after purification in yields ranging from 44 to 86% (Table 3, entries 1–7).

Then, we prepared **10ci**, an analogue of **10bi** in which the 3-pyridyl group at C2 is replaced by 1-ethyl-5-imidazolyl (Table 3, bottom scheme). The idea was to verify whether the interaction between Lys85 and the nitrogen of the ring at C2 could be improved. Compound **10ci** was prepared similarly (Table 3, entry 8), and its structure was identified unambiguously by X-ray diffraction (see the ORTEP diagram in Fig. 2).

The inhibitory activities of these new compounds were evaluated for different kinases as mentioned previously and compared with those of **10ba** and **10bb** (Table 4). In addition, the dose-dependent effects of the most promising compounds were tested on GSK3 β and GSK3 α ; the corresponding IC₅₀ values are given in Table 5. Most of the derivatives lost their activities against GSK3, except compounds **10bg** and **10bi**

Table 3 Synthesis of 2,8-disubstituted oxazolo[5,4-*f*]quinoxalines **10bc–bi** and **10ci**



Entry	Product	X	Yield (%)
1	10bc		76
2	10bd		86
3	10be		76
4 ^a	10bf		44
5	10bg		78
6	10bh		49
7	10bi		83
8	10ci	—	67

^a **10bf** was prepared from **10be** (see the ESI†).

Table 4 Inhibitory activities of the optimized compounds against a short panel of disease-related protein kinases. The table displays the remaining kinase activities detected after treatment with 10 μ M of the tested compounds. The values obtained after treatment with 1 μ M are given in brackets. Results are expressed in % of maximal activity, i.e. measured in the absence of the inhibitor but with an equivalent dose of DMSO (solvent of the tested compounds). ATP concentration used in the kinase assays was 10 μ M L⁻¹ (values are mean values, $n = 2$). Kinases are from human origin unless specified: Mm, *Mus musculus*; Rn, *Rattus norvegicus*; Ssc, *Sus scrofa domestica*

Compd.	CDK2/CyclinA	CDK5/p25	CDK9/CyclinT	PIM1	RnDYRK1A	GSK3 α	GSK3 β	SscGSK3 α/β	CK1 ϵ	SscCK1 δ/ϵ	Haspin
10ba	—	66 (98)	27 (45)	23 (43)	3 (11)	9 (9)	2 (2)	—	65 (75)	—	12 (23)
10bb	≥ 100 (≥ 100)	93 (≥ 100)	7 (35)	20 (57)	—	2 (4)	6 (6)	16 (16)	53 (≥ 100)	72 (88)	24 (29)
10bc	—	77 (97)	31 (82)	86 (79)	3 (41)	11 (19)	≤ 0 (15)	—	69 (≥ 100)	—	30 (77)
10bd	—	67 (69)	29 (69)	29 (80)	14 (25)	≤ 0 (≤ 0)	10 (16)	—	51 (84)	—	26 (64)
10be	—	76 (≥ 100)	30 (69)	≥ 100 (≥ 100)	8 (51)	9 (9)	3 (13)	—	74 (96)	—	43 (54)
10bf	—	63 (84)	1 (4)	46 (≥ 100)	16 (28)	4 (11)	2 (9)	—	11 (46)	—	7 (16)
10bg	—	58 (97)	11 (40)	13 (≥ 100)	4 (21)	11 (13)	1 (5)	—	83 (93)	—	21 (58)
10bh	—	98 (87)	10 (49)	87 (≥ 100)	2 (30)	1 (8)	5 (20)	—	56 (85)	—	10 (44)
10bi	—	53 (99)	4 (69)	18 (≥ 100)	5 (19)	≤ 0 (≤ 0)	21 (14)	—	44 (86)	—	8 (63)
10ci	—	47 (95)	9 (26)	12 (40)	4 (24)	2 (5)	8 (9)	—	78 (≥ 100)	—	16 (48)

which behaved similar to **10ba** against GSK3 β , but showed potency towards GSK3 α . It is worth noting that in spite of similar ring sizes, increasing activities are noticed from **10ba** to **10bg** and **10bi**, suggesting that either conformational changes or additional interactions might occur with these latter compounds. Finally, the dose-dependent effect of **10ba**, **10bg**, **10bi** and **10ci** was determined on DYRK1A, which showed a rather good preference of these inhibitors for GSK3 when compared with DYRK1A.

Conclusions

These results allowed us to identify the oxazolo[5,4-*f*]quinoxalines **10ba**, **10bg** and **10bi** as strong ATP-competitive inhibitors of GSK3. The most potent GSK3 inhibitors reported in the literature are pyrimidine **CHIR 98014**¹⁴ and bis(aryl)maleimide **LY2090314**,¹⁵ which have subnanomolar or nanomolar IC₅₀ values (Fig. 5, left; Table 5, entries 14 and 15); however, while **CHIR 98014** selectively inhibits GSK3 β , **LY2090314** binds almost equally to GSK3 α and GSK3 β . In contrast, while inhibitors with high isoform-selectivity for GSK3 α exist (e.g. **BRD0705**¹⁶ and **G28_14**¹⁷ with IC₅₀(GSK3 β)/IC₅₀(GSK3 α) ratios of 7.8 and 6.6, respectively), they are less potent (Fig. 5, right; Table 5, entries 16 and 17). Our best inhibitor, the sulphur-containing molecule **10bi** is potent and it binds GSK3 α more easily than GSK3 β (ratio of 4.6). Thus, it will be a subject of further studies aimed at identifying potent and selective inhibitors of GSK3 α . It is indeed of interest to identify isoform-selective kinase inhibitors for the development of new therapies.¹⁷ Efforts devoted to cellular testing in order to identify and develop applications for this new family of heterocycles are also ongoing in the lab.

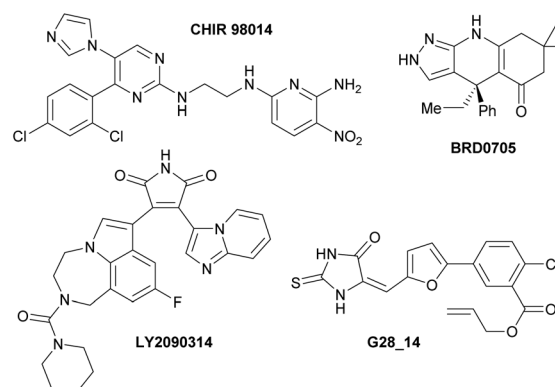


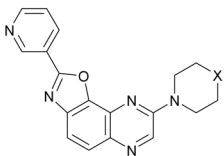
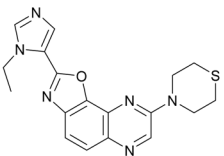
Fig. 5 Left: Potent inhibitors of GSK3 α/β **CHIR 98014**¹⁴ and **LY2090314**.¹⁵ Right: Selective inhibitors of GSK3 α vs. GSK3 β **BRD0705**¹⁶ and **G28_14**.¹⁷

Experimental section

Procedure used to convert **12b** into **10bi**

To a suspension of iodinated amide **12b** (0.41 g, 1.0 mmol) in dry DMSO (4 mL) were added thiomorpholine (0.11 mL,

Table 5 IC₅₀ values (nM) for the most promising inhibitors of GSK3^a

<div style="display: flex; justify-content: space-around; align-items: center;"> <div style="text-align: center;">  <p>10ba-bi</p> </div> <div style="text-align: center;">  <p>10ci</p> </div> </div>						
Entry	Product	X	GSK3 α	GSK3 β	^b	RnDYRK1A
1	10ba	O	15	25	1.7	200
2	10bb	N-Me	24	55	2.3	—
3	10bc	N-Benzyl	40	102	2.55	—
4	10bd	N-CH ₂ -5-(1,3-benzodioxolyl)	88	127	1.4	—
5	10be	N-Boc	57	97	1.7	—
6	10bf	N-H	24	68	2.8	—
7	10bg	CH ₂	11	33	3.0	390
8	10bh	CH-morpholino	22	35	1.6	—
9	10bi	S	4.8	22	4.6	130
10	10ci	—	31	50	1.6	447
11	Indirubine-3'-monoxime	72	55 (22) ^{c,11}	0.76	—	—
12	Hymenialdisine	3.6	10 (10) ^{c,12}	2.8	—	—
13	Alsterpaullone	30 (4) ^{c,13}	22 (4) ^{c,13}	0.73	—	—
14 ¹⁴	CHIR 98014	7.0	0.6	0.09	—	—
15 ¹⁵	LY2090314	1.5	0.9	0.60	—	—
16 ¹⁶	BRD0705	66	515	7.8	—	—
17 ¹⁷	G28_14	33	218	6.6	—	—

^a Three known inhibitors (indirubine-3'-monoxime, hymenialdisine and alsterpaullone) were also measured as controls. Values obtained from the literature for known potent or selective inhibitors were also added for comparison. ^b IC₅₀(GSK3 β)/IC₅₀(GSK3 α) as an evaluation of the isoform selectivity. ^c Values obtained from the literature (radioactive method using 15 μ M ATP).

1.1 mmol) and potassium carbonate (0.29 g, 2.2 mmol). After stirring at room temperature for 1 h, copper(i) iodide (19 mg, 0.10 mmol) was added. The tube was sealed, heated at 110 °C for 12 h and then cooled. The resulting dark mixture was poured into cold water (20 mL); the precipitate was filtered, washed with cold water (5 mL) and dissolved in chloroform. The organic layer was dried over sodium sulphate and the solvent was removed under reduced pressure. The product was purified by chromatography over silica gel (eluent: CHCl₃–MeOH 97 : 3).

Kinetic studies

Kinetic experiments were performed by varying the concentrations of ATP (from 1 to 100 μ M) and inhibitor **10bb** (0.05 and 0.02 μ M), while the concentration of the substrate GS2 was kept constant (12.5 μ M). The ADP-Glo kinase assay¹⁸ was used. Double-reciprocal plotting of the data is depicted in Fig. 3.

Docking studies

Before the docking studies, ligands and targets need to be pre-processed. Ligands were prepared for docking using the LigPrep tool,¹⁹ using the OPLS2005 force field, and by calculating the protonation state at pH = 7.2 \pm 0.2. For target pre-processing, the Maestro Protein Preparation Wizard²⁰ was used. The crystallographic structure of GSK3 β in a complex with a known inhibitor (PDBID 4ACD)²¹ was preprocessed by adding hydrogen atoms, removing the counterions and water mole-

cules, and protonating the residues at pH = 7.2. To develop the docking studies, we used Glide²² to perform the docking calculations using the Extra Precision Glide mode. The innerbox size of the grid was 16 \times 16 \times 16 Å and the outerbox size was 33.5 \times 33.5 \times 33.5 Å. The grid box was centred on coordinates 0.432, 9.255, 31.434, that correlate with the centre of the ATP-binding site. 10 poses per ligand were calculated and classified by the binding energy. To validate the docking protocol, we employed some GSK3 β inhibitors with a known binding mode to the ATP-binding site of the enzyme.^{16,22,23}

Conflicts of interest

There are no conflicts to declare.

Acknowledgements

We thank the Université de Rennes 1 and the Centre National de la Recherche Scientifique for supporting this research. We acknowledge the support from the Fonds Européen de Développement Régional (FEDER; D8 VENTURE Bruker AXS diffractometer). A. M. acknowledges financial support from Spanish Ministry of Innovation, Science and Universities (MICU, grant no. SAF2016-76693-R) and ISCiii (CIBERNED, grant no. CB18/05/00040). S. B. and S. R. also thank the Cancéropôle Grand Ouest (axis: Natural Sea Products in Cancer Treatment), IBISA (French *Infrastructures en sciences du*

vivant: biologie, santé et agronomie) and Biogenouest (Western France Life Science and Environment Core Facility Network) for supporting KISSf screening facility. We also thank Aurélie Assicot for her contribution to the study and Ludovic Paquin for the generous gift of secondary amines.

Notes and references

- 1 T. Eicher, S. Hauptmann and A. Speicher, *The Chemistry of Heterocycles: Structure, Reactions Synthesis and Applications*, Wiley-VCH, Weinheim, 2nd edn, 2003.
- 2 J. H. Musser, H. Jones, S. Sciortino, K. Bailey, S. M. Coutts, A. Khandwala, P. Sonnino-Goldman, M. Leibowitz, P. Wolf and E. S. Neiss, *J. Med. Chem.*, 1985, **28**, 1255.
- 3 J. Deng, E. Feng, S. Ma, Y. Zhang, X. Liu, H. Li, H. Huang, J. Zhu, W. Zhu, X. Shen, L. Miao, H. Liu, H. Jiang and J. Li, *J. Med. Chem.*, 2011, **54**, 4508.
- 4 (a) N. Mokhtari Brikci-Nigassa, G. Bentabed-Ababsa, W. Erb, F. Chevallier, L. Picot, L. Vitek, A. Fleury, V. Thiery, M. Souab, T. Robert, S. Ruchaud, S. Bach, T. Roisnel and F. Mongin, *Tetrahedron*, 2018, **74**, 1785; (b) N. Mokhtari Brikci-Nigassa, L. Nauton, P. Moreau, O. Mongin, R. E. Duval, L. Picot, V. Thiéry, M. Souab, S. Ruchaud, S. Bach, R. Le Guevel, G. Bentabed-Ababsa, W. Erb, T. Roisnel, V. Dorcet and F. Mongin, *Bioorg. Chem.*, 2019, **82**, DOI: 10.1016/j.bioorg.2019.103347.
- 5 G. Evindar and R. A. Batey, *J. Org. Chem.*, 2006, **71**, 1802.
- 6 X. Hui, J. Desrivot, C. Bories, P. M. Loiseau, X. Franck, R. Hocquemiller and B. Figadère, *Bioorg. Med. Chem. Lett.*, 2006, **16**, 815.
- 7 (a) W. R. Bowman, H. Heaney and P. H. G. Smith, *Tetrahedron Lett.*, 1982, **23**, 5093; (b) T. Minami, T. Isonaka, Y. Okada and J. Ichikawa, *J. Org. Chem.*, 1993, **58**, 7009; (c) B. A. Lanman, V. J. Cee, S. R. Cheruku, M. Frohn, J. Golden, J. Lin, M. Lobera, Y. Marantz, K. M. Muller, S. C. Neira, A. J. Pickrell, D. Rivenzon-Segal, N. Schutz, A. Sharadendu, X. Yu, Z.-D. Zhang, J. Buys, M. Fiorino, A. Gore, M. Horner, A. Itano, M. McElvain, S. Middleton, M. Schrag, H. M. Vargas, H. Xu, Y. Xu, X.-X. Zhang, J. Siu and R. W. Burli, *ACS Med. Chem. Lett.*, 2011, **2**, 102; (d) J. Peng, C. Zong, M. Ye, T. Chen, D. Gao, Y. Wang and C. Chen, *Org. Biomol. Chem.*, 2011, **9**, 1225; (e) J.-H. Jia, C.-L. Jiang, X.-J. Zhang, Y.-W. Jiang and D.-W. Ma, *Tetrahedron Lett.*, 2011, **52**, 5593; (f) V. Kavala, D. Janreddy, M. J. Raihan, C.-W. Kuo, C. Ramesh and C.-F. Yao, *Adv. Synth. Catal.*, 2012, **354**, 2229; (g) P. J. Tambade, Y. P. Patil, Z. S. Qureshi, K. P. Dhake and B. M. Bhanage, *Synth. Commun.*, 2012, **42**, 176; (h) A. Ahmed, R. Singha and J. K. Ray, *Tetrahedron Lett.*, 2015, **56**, 2167; (i) T. Venu Saranya, P. Rajan Sruthi and S. Anas, *Synth. Commun.*, 2019, **49**, 297.
- 8 S. Klaeger, S. Heinzlmeir, M. Wilhelm, H. Polzer, B. Vick, P.-A. Koenig, M. Reinecke, B. Ruprecht, S. Petzoldt, C. Meng, J. Zecha, K. Reiter, H. Qiao, D. Helm, H. Koch, M. Schoof, G. Canevari, E. Casale, S. R. Depaolini, A. Feuchtinger, Z. Wu, T. Schmidt, L. Rueckert, W. Becker, J. Huenges, A.-K. Garz, B.-O. Gohlke, D. P. Zolg, G. Kayser, T. Vooder, R. Preissner, H. Hahne, N. Tonisson, K. Kramer, K. Goetze, F. Bassermann, J. Schlegl, H.-C. Ehrlich, S. Aiche, A. Walch, P. A. Greif, S. Schneider, E. R. Felder, J. Ruland, G. Medard, I. Jeremias, K. Spiekermann and B. Kuster, *Science*, 2017, **358**, 1148.
- 9 (a) R. Roskoski Jr., *Pharmacol. Res.*, 2019, **144**, 19; (b) H. L. Lightfoot, F. W. Goldberg and J. Sedelmeier, *ACS Med. Chem. Lett.*, 2019, **10**, 153.
- 10 (a) M. K. Pandey and T. R. DeGrado, *Theranostics*, 2016, **6**, 571; (b) A. P. Saraswati, S. M. Ali Hussaini, N. H. Krishna, B. N. Babu and A. Kamal, *Eur. J. Med. Chem.*, 2018, **144**, 843.
- 11 S. Leclerc, M. Garnier, R. Hoessel, D. Marko, J. A. Bibb, G. L. Snyder, P. Greengard, J. Biernat, Y.-Z. Wu, E.-M. Mandelkow, G. Eisenbrand and L. Meijer, *J. Biol. Chem.*, 2001, **276**, 251.
- 12 L. Meijer, A. M. W. H. Thunnissen, A. W. White, M. Garnier, M. Nikolic, L. H. Tsai, J. Walter, K. E. Cleverley, P. C. Salinas, Y. Z. Wu, J. Biernat, E. M. Mandelkow, S. H. Kim and G. R. Pettit, *Chem. Biol.*, 2000, **7**, 51.
- 13 M. Leost, C. Schultz, A. Link, Y.-Z. Wu, J. Biernat, E.-M. Mandelkow, J. A. Bibb, G. L. Snyder, P. Greengard, D. W. Zaharevitz, R. Gussio, A. M. Senderowicz, E. A. Sausville, C. Kunick and L. Meijer, *Eur. J. Biochem.*, 2000, **267**, 5983.
- 14 A. S. Wagman, R. S. Boyce, S. P. Brown, E. Fang, D. Goff, J. M. Jansen, V. P. Le, B. H. Levine, S. C. Ng, Z.-J. Ni, J. M. Nuss, K. B. Pfister, S. Ramurthy, P. A. Renhowe, D. B. Ring, W. Shu, S. Subramanian, X. A. Zhou, C. M. Shafer, S. D. Harrison, K. W. Johnson and D. E. Bussiere, *J. Med. Chem.*, 2017, **60**, 8482.
- 15 J. M. Atkinson, K. B. Rank, Y. Zeng, A. Capen, V. Yadav, J. Manro, T. A. Engler and M. Chedid, *PLoS One*, 2015, **10**, e0125028/1.
- 16 F. F. Wagner, L. Benajiba, A. J. Campbell, M. Weiewer, J. R. Sacher, J. P. Gale, L. Ross, A. Puissant, G. Alexe, A. Conway, M. Back, Y. Pikman, I. Galinsky, D. J. Deangelo, R. M. Stone, T. Kaya, X. Shi, M. B. Robers, T. Machleidt, J. Wilkinson, O. Hermine, A. Kung, A. J. Stein, D. Lakshminarasimhan, M. T. Hemann, E. Scolnick, Y.-L. Zhang, J. Q. Pan, K. Stegmaier and E. B. Holson, *Sci. Transl. Med.*, 2018, **10**, eaam8460/1.
- 17 Y. Wang, X. Dou, L. Jiang, H. Jin, L. Zhang, L. Zhang and Z. Liu, *Eur. J. Med. Chem.*, 2019, **171**, 221.
- 18 ADP-Glo™ Kinase Assay Technical Manual: [https://www.promega.es/resources/protocols/technical-manuals/0/adp-glo-kinase-assay-protocol/\(July 30, 2019\)](https://www.promega.es/resources/protocols/technical-manuals/0/adp-glo-kinase-assay-protocol/(July 30, 2019)).
- 19 *Schrödinger Release 2016-4: LigPrep*, Schrödinger, LLC, New York, NY, 2019.
- 20 M. G. Sastry, M. Adzhigirey, T. Day, R. Annabhimoju and W. Sherman, *J. Comput. Aided Mol. Des.*, 2013, **27**, 221.
- 21 S. Berg, M. Bergh, S. Hellberg, K. Högdin, Y. Lo-Alfredsson, P. Söderman, S. von Berg, T. Weigelt, M. Örmö, Y. Xue,

- J. Tucker, J. Neelissen, E. Jerning, Y. Nilsson and R. Bhat, *J. Med. Chem.*, 2012, **55**, 9107.
- 22 R. A. Friesner, R. B. Murphy, M. P. Repasky, L. L. Frye, J. R. Greenwood, T. A. Halgren, P. C. Sanschagrin and D. T. Mainz, *J. Med. Chem.*, 2006, **49**, 6177.
- 23 (a) S. H. Liang, J. M. Chen, M. D. Normandin, J. S. Chang, G. C. Chang, C. K. Taylor, P. Trapa, M. S. Plummer, K. S. Para, E. L. Conn, L. Lopresti-Morrow, L. F. Lanyon, J. M. Cook, K. E. G. Richter, C. E. Nolan, J. B. Schachter, F. Janat, Y. Che, V. Shanmugasundaram, B. A. Lefker, B. E. Enerson, E. Livni, L. Wang, N. J. Guehl, D. Patnaik, F. F. Wagner, R. Perlis, E. B. Holson, S. J. Haggarty, G. El Fakhri, R. G. Kurumbail and N. Vasdev, *Angew. Chem., Int. Ed.*, 2016, **55**, 9601; (b) F. F. Wagner, L. Benajiba, A. J. Campbell, M. Weiewer, J. R. Sacher, J. P. Gale, L. Ross, A. Puissant, G. Alexe, A. Conway, M. Back, Y. Pikman, I. Galinsky, D. J. Deangelo, R. M. Stone, T. Kaya, X. Shi, M. B. Robers, T. Machleidt, J. Wilkinson, O. Hermine, A. Kung, A. J. Stein, D. Lakshminarasimhan, M. T. Hemann, E. Scolnick, Y.-L. Zhang, J. Q. Pan, K. Stegmaier and E. B. Holson, *Sci. Transl. Med.*, 2018, **10**, eaam8460/1; (c) F. X. Tavares, J. A. Boucheron, S. H. Dickerson, R. J. Griffin, F. Preugschat, S. A. Thomson, T. Y. Wang and H.-Q. Zhou, *J. Med. Chem.*, 2004, **47**, 4716.